Available online at www.sciencedirect.com

ScienceDirect

Ceramics International 40 (2014) 3517–3525

CERAMICS INTERNATIONAL

www.elsevier.com/locate/ceramint

Effects of manufacturing conditions and heating on properties of electrochemically produced magnetite nano-powders

D. Mamula-Tartalja[a], Lj. Vulićević[b], I. Radisavljević[c], M. Mitrić[c], V. Andrić[c], B. Kuzmanović[c], M. Medić[c], N. Ivanović[c,*]

[a]*Higher Education School of Professional Studies for Information and Communication Technologies, Zdravka Čelara 16, 11000 Belgrade, Serbia*
[b]*Technical Faculty Čačak, University of Kragujevac, Svetog Save 65, 32000 Čačak, Serbia*
[c]*"Vinča" Institute of Nuclear Sciences, University of Belgrade, POB 522, 11001 Belgrade, Serbia*

Received 13 June 2013; received in revised form 22 August 2013; accepted 16 September 2013
Available online 25 September 2013

Abstract

Electrochemical (EC) synthesis of magnetite (Fe_3O_4) nano-powders of specific characteristics is investigated in the range of current densities of $J=200$–$1000\ \mathrm{mA/dm^2}$, and temperatures of $T=295$–361 K. The obtained powders and their modification upon heating in air and argon atmosphere are examined by X-ray diffraction (XRD), scanning electron microscopy (SEM), transmition electron microscopy (TEM), laser light scattering particle size distribution measurements, magnetic measurements by Faraday method and SQUID, and measurements of specific electrical resistivity. It has been established that structure, morphology, magnetic and electrical properties of the powders can be adjusted by using adequate EC synthesis conditions, and/or by their subsequent heating in the appropriate atmosphere. The temperature induced magnetite reordering, the magnetite to maghemite (γ-Fe_2O_3), and the maghemite to haematite (α-Fe_2O_3) phase transitions were examined, too.
© 2013 Elsevier Ltd and Techna Group S.r.l. All rights reserved.

Keywords: A. Annealing; A. EC synthesis; B. Magnetite nanopowders; B. Structure; C. Properties

1. Introduction

The fact that many of their properties differ from those of bulk materials makes magnetic iron oxides nano-particles interesting from both practical and theoretical point of view [1–3]. Below a critical dimension, which is typically around 100 nm, they consist of a single magnetic domain (SD), and smaller particles can exhibit super-paramagnetic (SPM) behaviour [4]. They are extensively used as components of ferro fluids, biomedical materials [5], and catalysts [6], or for magnetic recording [1,6]. Moreover, the relationship between structure and magnetic properties of iron oxides, and their evolution upon heating in various atmospheres is of great importance in geophysics [7,8], archaeology [9], and for understanding of the rusting process [10].

Magnetite and maghemite have similar inverse spinel face centred cubic (fcc) structure and magnetic properties, but maghemite is chemically and thermally more stable, and has considerably higher electrical resistivity [4]. They can be represented by the single formula [7]: $(Fe^{3+})_A[Fe^{2+}_{1-y}\,Fe^{3+}_{1+y/3}\,\square_{y/3}]_BO_4$, where A denotes tetrahedral (8a), and B octahedral (16d) crystallographic position, $\square$-vacancies, $0\leq y\leq 1$, $y=0$ gives pure magnetite, and $y=1$ pure maghemite. However, the role of cations and vacancies (C–V) reordering in magnetite to maghemite phase transition, and properties of the involved intermediate phases are not fully understood [11,12]. Except from ores, magnetite can be produced by chemical [13], biological [14] and micro-emulsion [15] methods. Stoichiometry, C–V distribution and ordering, and the presence of particular impurities and defects are highly dependent on the synthesis route and the sample history, strongly influencing its structure, electronic and magnetic properties [16].

A growing interest for electrochemical (EC) methods of iron oxides powders synthesis [17,18,19] has motivated the presented investigation whose intention was to relate the EC synthesis conditions to the grain size and distribution, particle shape, electrical and magnetic properties of the obtained powders, and

---

*Corresponding author. Tel.: +381 11 3408 434; fax: +381 11 3400 100.
E-mail addresses: danica.mamula@ict.edu.rs (D. Mamula-Tartalja), nivanov@vin.bg.ac.rs (N. Ivanović).

0272-8842/$ - see front matter © 2013 Elsevier Ltd and Techna Group S.r.l. All rights reserved.
http://dx.doi.org/10.1016/j.ceramint.2013.09.077

to examine their behaviour during subsequent heating in argon and in air. In addition, thermal evolution of magnetite, its oxidation, the magnetite to maghemite, and the maghemite to haematite phase transitions are addressed by measuring the changes of magnetic susceptibility and specific electrical resistivity during non-isothermal heating of the powders in air and argon atmosphere.

2. Experimental

The investigated powders were produced in the EC cell at temperatures between 295 (*RT*) and 361 K, and current densities between J=200 and 1000 mA/dm^2 using the 0.04 normal NaCl solution in deionised water as electrolyte. The two rectangular steel plates with low carbon content (∼99.6 mass% of Fe, with maximum 0.25 mass% of Mn as the main impurity) separated for 3 cm, were used as electrodes. Synthesis was conducted for 30–60 min to produce a sufficient amount of powders without significant change of the starting $pH \approx 5.5$ of the electrolyte. XRD measurements were performed using the nickel-filtered CuK_α radiation (λ=1.5418 Å) from a PW 1130 Phillips X-ray generator operating at 40 kV, coupled to a Phillips X-ray diffractometer with a PW 1710 controller. SEM micrographs were obtained with a JOEL, JSM-35 device, using a 25 keV electron beam energy at zero tilt angle. TEM micrographs were attained by a Phillips EM 400 instrument operating at 120 kVm, with samples deposited on a carbon coated Cu grid. After a 10 min treatment in the ultrasound bath, the size distribution of the powders was measured in deionised water, at RT, by a MALVERN Mastersizer 2000 laser light scattering particle size analyser. Magnetisation as function of external magnetic field was measured by a "Quantum Design" MPMS XL-5 SQUID magnetometer, at RT. The temperature dependence of magnetic susceptibility $\chi(T)$ was measured by the modified Faraday method [20] under magnetic field intensity of H=5440 A/m, (68 Oe) in the temperature range from *RT* to ∼900 K. Direct current (DC) specific electrical resistivity $\rho(T)$ was measured in the temperature range from *RT* to ∼600 K, using an in-house built electrometer. Cylindrical samples used for $\chi(T)$ and $\rho(T)$ measurements were produced by pressing the powders uniaxially from the two-sides under 400 MPa, and measurements were performed in air and argon atmosphere under non-isothermal conditions (heating/cooling rate of 25 K min^{-1}).

3. Results

The principle reactions taking place during the EC synthesis are [17–19]:

$$\text{Anode: } Fe^{3+} + 3OH \leftrightarrow (\gamma \text{ and/or } \alpha)\text{-}FeOOH + H_2O \qquad (1)$$

$$2H_2O \leftrightarrow 4H^+ + 4e^- + O_2 \qquad (1a)$$

Table 1
The EC synthesis conditions (J, T), and some structural parameters of the investigated magnetite powders.

Sample	J [mA/dm^2]	T [K]	d_{cr} [nm]	a [Å]	ΔV [Å^3]	$y/3$ [nm]	n_{vac} [nm]
1	200	293	8	8.364	6.95	0.216	1.7
2	200	313	12	8.368	6.11	0.190	1.5
3	200	333	18 10–30^a	8.35	9.89	0.307	2.5
4	200	361	34	8.396	1. 90	0.059	0.5
5	300	333	24	8.369	5.90	0.183	1.5
6	500	333	18	8.32	16.1	0.503	4
7	1000	333	20 15–30^a	8.37	5.70	0.176	1.4
8	1000	361	21 10–30^a	8.384	2.75	0.085	0.7

Crystallite size d_{cr}, and lattice constant a are determined from XRD measurements. $\Delta V = a^3_{mgn} - a^3$ (a_{mgn}=8.397 Å, JCPDS 19-629) is the experimentally observed unit cell contraction of magnetite lattice. The numbers of vacancies $n_{vac} = \Delta V/\Delta V_p$, $\Delta V_p = a^3_{mgn} - a^3_{mgh}$, and the cation deficiency parameter $y/3$ [11] are estimated using a_{mgh}=8.346 Å (JCPDS 39-1346) for maghemite lattice constant.

[a] TEM results [21].

Table 2
Some atomic and structural parameters relevant for magnetite and maghemite structure.

Coordination	$d_{Fe\text{–}O}$ [Å]	$R_{Fe^{3+}}$ [Å]	$R_{Fe^{2+}}$ [Å]	$\Delta V_{tet^{3+}}$ [Å^3]	$\Delta V_{oct^{3+}}$ [Å^3]	$\Delta V_{oct^{2+}}$ [Å^3]
Tetrahedral	#1.857	0.49 #0.457	0.63	0.37 #0.277		
Octahedral	#2.077	0.645(HS) 0.55(LS) #0.609	0.78(HS) 0.61(LS) #0.745		0.332 0.095 #0.154	1.196 0.159 #0.940

$d_{Fe\text{–}O}$=1.99 Å is "critical" value of the octahedral Fe–O bond length that leads to insulator-to-metal phase transition [22]. $d_{O\text{–}O}$=2.80 Å is the ideal O–O bond length assuming the oxygen ionic radius of $R_{O^{2-}}$ = 1.40 Å [23].

$R_{Fe^{3+}}$, and $R_{Fe^{2+}}$, are ionic radii of iron from Reference [24], (HS) – high spin, (LS) – low spin values.

#1.857,#2.077 are $d_{Fe\text{–}O}$ distances experimentally obtained for sample 4 with the best defined crystal structure among the investigated samples. Corresponding #hash;$R_{Fe^{3+}}$ and #hash;$R_{Fe^{2+}}$ values are determined from the bond lengths assuming that magnetite has an ideal inverse spinel structure, and $R_{O^{2-}}$ = 1.40 Å. R_{tet}=0.308 Å, and R_{oct}=0.574 Å are radii of tetrahedral and octahedral vacancy, respectively, for $R_{O^{2-}}$ = 1.40 Å [25]. $\Delta V_{tet^{3+}}$, $\Delta V_{oct^{2+}}$, and $\Delta V_{oct^{3+}}$ are the lattice expansions due to the volume differences between the volumes of Fe^{3+} and Fe^{2+}, and to them available vacancies.

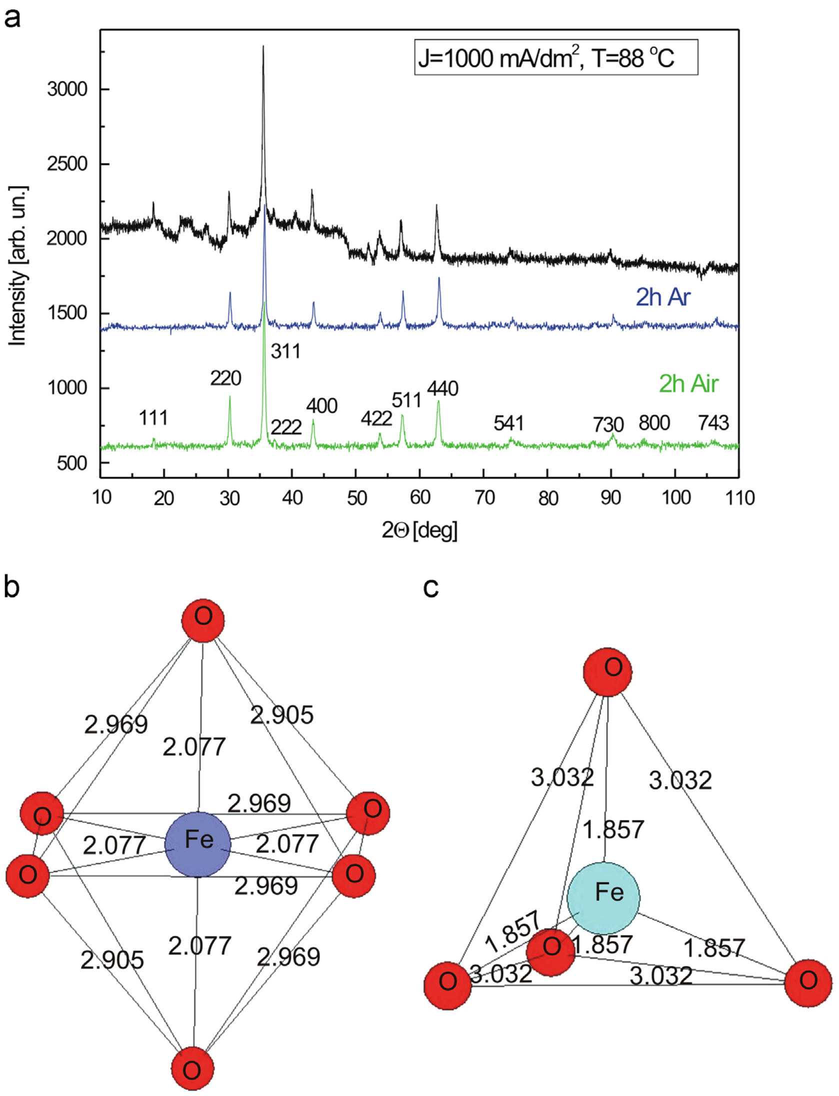

Fig. 1. (a) XRD patterns of sample 8: as synthesised (1), after isothermal heating at 553 K for 2 h in argon (2), and in air (3); (b) bond lengths in sample 4 at 16d, (c) at 8a crystallographic position.

Cathode: $H_2O + e^- \leftrightarrow 1/2H_2 + OH^-$ (2)

Solution: $3(\gamma \text{ and/or } \alpha)\text{-FeOOH} + 1/2H_2 \rightarrow Fe_3O_4 + 2H_2O$ (3)

The synthesis conditions and some structural parameters of the obtained powders are presented in Table 1.

Some additional parameters useful for understanding magnetite and maghemite structures are given in Table 2.

XRD patterns of sample 8, as synthesised at $T = 361$ K and $J = 1000$ mA/dm^2 (1), after its thermal treatment in argon (2), and in air atmosphere (3), are given in Fig. 1(a), and the bond lengths of sample 4 in Fig. 1(b) (16d position), and Fig. 1(c) (8a position).

Two hours of heating at 553 K in argon improves the initial crystal structure of the sample considerably, and this structural improvement is most likely accompanied by the heating induced C–V redistribution. After heating the sample for two hours at 553 K in air, the maghemite phase has been formed, according the reaction:

$4Fe_3\ O_4 + O_2 \rightarrow 6\gamma\text{-}Fe_2O_3$ (4)

which is particularly effective above 550 K [12,26]. The oxygen sub-lattice does not change significantly during this process, so the spinel structure of magnetite is preserved, but all Fe ions go into the Fe^{3+} state, and their number per unit cell reduces from 24 in magnetite to $21^1/_3$ in maghemite, so maghemite can be thought of as the fully oxidised magnetite [27].

SEM micrographs of sample 1 (Fig. 2(a)), and sample 7 (Fig. 2(b)), and TEM micrographs of sample 8 (Fig. 2(c) and (d)) show the existence of two phases with entirely different dimensions and grain morphology.

One phase consists of large, regularly shaped, plate-like (PL) grains with diameter ranging from 300 nm to 800 nm. This phase is most likely formed from the plate-like lepidocrocite (γ-FeOOH) crystals, which, with help of hydrogen from electrolyte quickly transforms into tabular magnetite. The other phase is formed from the goethite (α-FeOOH) precursor. This phase, made of needle-like

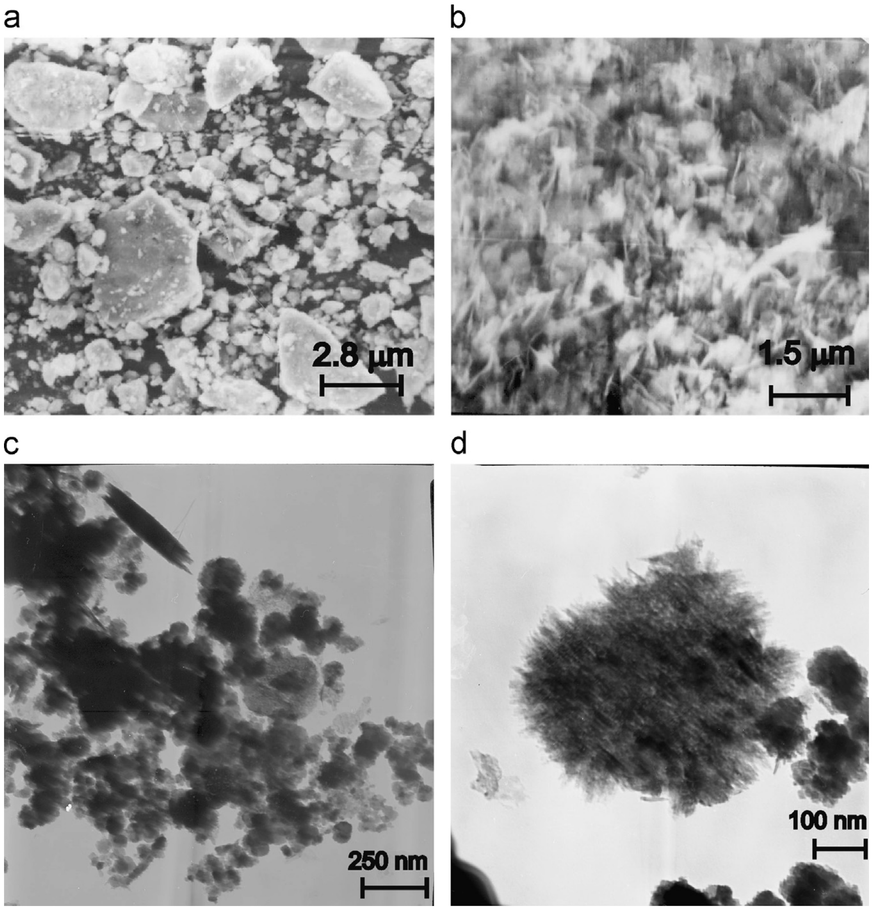

Fig. 2. SEM micrographs of sample 1 (a), and sample 7 (b), and TEM micrographs of sample 8 (c) and (d).

crystallites (whiskers, WH) with diameter ranging from 15 to 80 nm and their bundles, preserves the initial morphology. The additional information about the powders grain size distributions and morphology obtained by laser light scattering measurements are presented in Table 3.

Besides the two main types of particles mentioned above, in most of the samples there exists yet another type of particles comprising large agglomerates (LA) with dimensions of 5–5.5 μm.

The temperature dependences of normalised susceptibility, $\chi_N(T)=\chi_{RT}/\chi_T$, ($\chi_{RT}$ is the initial RT susceptibility, and χ_T is susceptibility at temperature T) of sample 8, obtained during non-isothermal heating/cooling cycles at the rate of ~25 K min^{-1} in air and in argon atmosphere are presented in Fig. 3(a and b), respectively.

$\chi_N(T)$ increases with T between RT and a maximum, which is placed around 600 K. After that, $\chi_N(T)$ decreases with T, and reaches zero at $T=893$ K in air (Fig. 3 (a)), and at $T=853$ K in argon (Fig. 3 (b)). Upon cooling the sample back to RT in air, χ_N recovers less than a half (1/2.3) of the initial value, indicating that heating in air produces a weak magnetic structure. The XRD pattern of sample 8, taken after 1.5 h (which is much longer than a typical $\chi_N(T)$ measurement takes ~40 min) of isothermal heating at 893 K in air is presented in Fig. 4.

Haematite (H-peaks) phase dominates, but small amount of γ-Fe_2O_3 (Mh-peaks) is still present, which explains weak magnetisation of the sample observed after the heating/cooling cycle in air.

Curie temperature T_C~893 K of the produced γ-Fe_2O_3 phase (Fig. 3(a)) is considerably larger than $T_C=848$ K derived from extrapolation of the Curie temperature of magnetite $T_C=853$ K [28,29], suggesting that a specific C–V ordering exists in the sample. After another heating/cooling procedure no magnetisation was observed in the sample implying that γ-Fe_2O_3 to α-Fe_2O_3 phase transition had been completed, and that a small amount of γ-Fe_2O_3 observed after the first cycle did not originate from α-Fe_2O_3 to γ-Fe_2O_3 transition, as thought possible under specific conditions [7].

During heating in argon $\chi_N(T)$ approaches zero in the vicinity of the Curie temperature of magnetite $T_C=853$ K, suggesting that magnetite phase has been preserved in the entire T interval. After cooling back to RT, the χ_{RT} reaches 2.5 times larger value than the initial one. This was confirmed in another sample in which χ_{RT} increased three times after the first heating/cooling cycle in argon.

RT magnetisation curves of sample 7 and sample 4 are presented in Fig. 5(a) and (b) respectively.

Table 3
Particle size distributions of the EC obtained magnetite powders measured by the laser light scattering method.

Sample	d [nm]	$\Delta d/d$ [%]	I [%]	d_{sf} [nm]	$\Delta d_{sf}/d_{sf}$ [%]	V [%]	$\lvert(d-d_{sf})/d\rvert$ [%]	Polydispersity
1	300	30.6	40.7	294	29.7	6.3	2	0.393
$J=200$	1180	36.6	57.4	1420	38.2	51.9	20.3	
(RT)	5240	8.6	1.9	5330	13.4	41.8	1.7	
2	171	21	42.8	144	21	9	16	0.825
$J=200$	1180	32	44	1360	33	12	15	
(313)	4950	13	13.2	5140	15	79	4	
3	181	22	78.8	149	23	30.0	18	0.511
$J=200$	940	23	17.2	994	25	7.3	6	
$T=333$	5400	6	4.1	5470	12	62.7	1	
4	160	23	77.0	135	21	36.0	16	0.497
$J=200$	916	25	17.9	978	26	5.7	7	
$T=361$	5310	7	5.1	5400	12	58.4	2	
5	1450	23	90.9	1590	25	32.8	10	0.355
$J=300$	5400	6	9.1	5470	12	67.2	1	
$T=333$								
6	212	40	88.3	148	45	43.1	30	0.263
$J=500$	2780	43	11.7	3970	32	56.9	43	
$T=333$								
7a	215	45	67.6	134	35	52.3	38	0.368
$J=1000$	938	46	31.4	1190	50	25	27	
RT	5060	11	1	5200	15	22.7	3	
7	258	40	56.8	141	28	13.5	45	0.423
$J=1000$	797	39	37.6	851	48	15.1	7	
$T=333$	5010	12	5.6	5190	15	71.4	4	
8	167	16	40.2	147	17	62.8	12	1
$J=1000$	469	17	59.8	488	20	37.2	4	
$T=361$								

d – the average dimension of a particle, d_{sf} – diameter of a spherical particle which produce the same signal as d-particle, $\Delta d/d$ and $\Delta d_{sf}/d_{sf}$ relative deviations of the particle size in a distribution, I – intensity of the signal obtained from the particular distribution, V – total volume of the particles in a distribution, $(d-d_{sf})/d$ – deviation of the particle average dimension from the corresponding spherical particle diameter ("asphericity").
SG distribution – the first row, IG distribution –the second row, LA distribution – the third row of each entry.

Saturation magnetisation M_S of bulk magnetite at RT is $M_{SB}\approx 92$ Am^2/kg, whereas bulk maghemite has $M_{SB}\approx 74$ Am^2/kg [16]. Hence, the measured values $M_{S7}\approx 47$ Am^2/kg and $M_{S4}\approx 76$ Am^2/kg confirm that M_S of iron oxides nanoparticles decreases rapidly with particle size [29–31]. In the investigated samples the decrease of the particle size and M_S is accompanied with increase of magnetic strength $\alpha=(1-M/Ms)H$ (α_4=0.52, α_7=1.34, for H taken in the saturation region of the hysteresis curve).

The $\rho(T)$ dependences of sample 8, measured during non-isothermal heating (25 K/min) in air and in argon, in the temperature range 293–600 K are given in Fig. 6.

Assuming that $\rho(T)$ follows the Arrhenius law $\rho(T)=\rho_o \exp(E_a/kT)$ [32] (where E_a is the activation energy, ρ_o is the high temperature resistivity, and $k=0.862\times10^{-4}$ eV K^{-1} is the Boltzmann constant), the activation energies determined from curves (I), (II), and (III) in Fig. 6 are estimated to be 0.98 eV, 0.68 eV and 0.23 eV, respectively. These values are comparable to previously reported experimental results [32–38], but considerably higher than 0.1 eV of a perfect, large Fe_3O_4 monocrystal [38].

4. Discussion

The presented investigation show that magnetite powders with grains of specific shape and properties can be produced by EC synthesis in the temperature interval $295\leq T\leq 363$ K, and current densities interval $200\leq J\leq 1000$ mA/dm^2, though in certain cases with a very small amount of maghemite. The results also confirm [18,19,39] that conditions imposed both to hydrogen and water during the EC process influence stability and characteristics of the magnetic iron oxide phases and consequently the final powder properties.

The difference between the lattice constants of "perfect" magnetite and maghemite is only about 5%, and their volume difference is V_p=10.723 Å^3 (Table 1). The number of vacancies in maghemite unit cell is $2^2/_3$ larger than in magnetite, and so the contribution of a single vacancy to the volume contraction should be $V_{vac}=4.021$ Å^3, which is much larger than the largest calculated value $\Delta V_{oct}^{2+}=1.196$ Å^3 in Table 2 (column 7). Evidently, more than a half of the structure relaxation during the magnetite to maghemite phase transformation is due to the causes other than that imposed by the

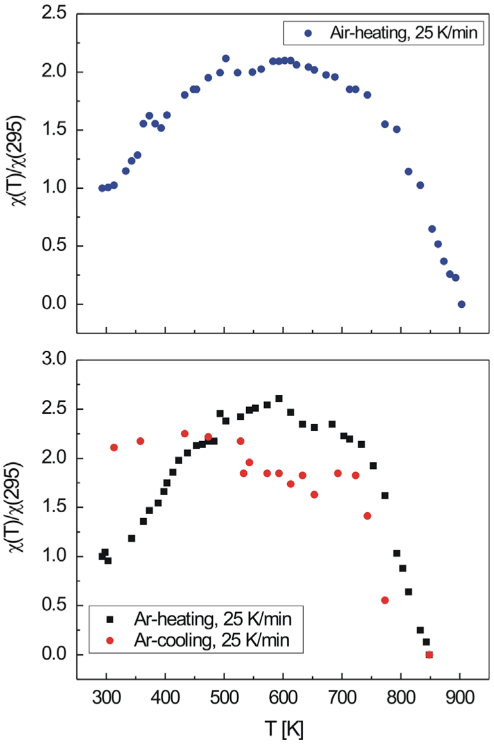

Fig. 3. Temperature dependence of normalised magnetic susceptibility $\chi_N(T)$ of sample 8, obtained during non-isothermal heating–cooling cycle at the rate of ~25 K min^{-1} in air (a), and in argon (b).

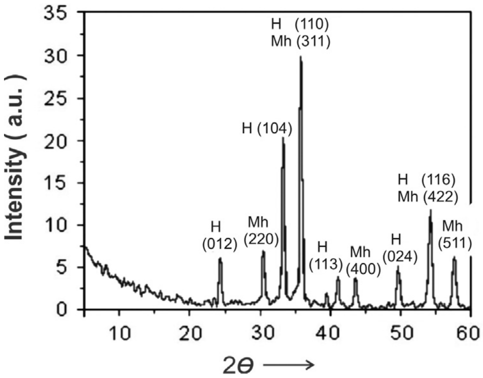

Fig. 4. XRD pattern of sample 8 after isothermal heating at 893 K for 1.5 h in air. H denotes α-Fe_2O_3, and Mh γ-Fe_2O_3 diffraction peaks.

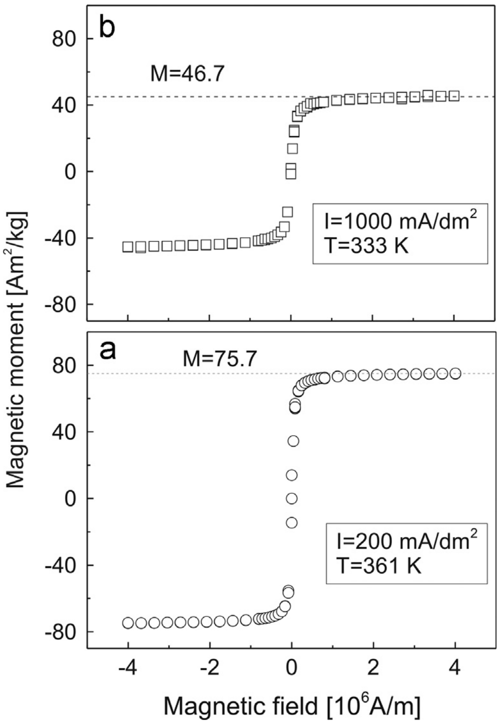

Fig. 5. Room temperature magnetisation curves of sample 7 (a), and sample 4 (b).

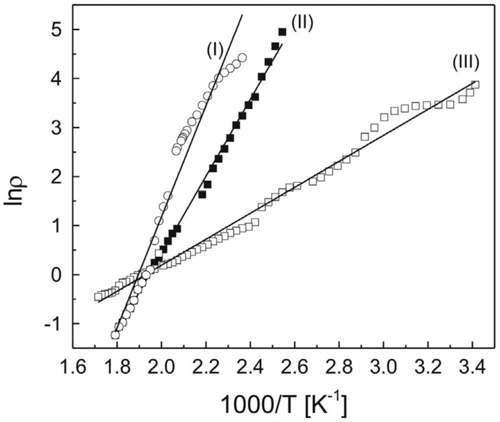

Fig. 6. Temperature dependence of electrical resistivity of sample 8 during non-isothermal heating in air (I); in argon, first (II), and in argon second (III) cycle.

geometrical mismatch between the Fe ions and the space in the crystal lattice available to them. Assuming $R_O^{2-}=1.40$ Å [23] and the typical distribution of cations in the inverse spinel structure of magnetite, the experimental value for the Fe–O bond at tetrahedral position ($^{\#}d_{Fe\text{–}O}=1.857$ Å – sample 4, 1.858 Å – sample 8) implies slightly smaller Fe^{3+} radius (row 2 in Table 2) and smaller volume expansion than the rigid-ion model predicts (row 1 in Table 2). At octahedral position ($^{\#}d_{Fe\text{–}O}=2.077$ Å – sample 4, 2.072 Å – sample 8) the experimentally observed Fe ionic radii lay in-between the literature LS and HS values [24], though somewhat closer to the HS values. This is especially true for Fe^{2+} ionic radius. It is obvious that at both crystallographic positions, none of the Fe ions has an integer valence. Smaller Fe ions closer to Fe^{3+} and in less perturbing LS state are favoured by the geometrical constrains of the lattice, whereas larger Fe ions in the HS configuration yield higher magnetic moments and are favoured by the magnetic interaction.

The results presented in Table 1 also indicate that under the investigated conditions, T influences the crystallite size during the EC synthesis more than J. For particular J, higher temperatures lead to formation of larger crystallites. For samples obtained at $J=200$ mA/dm^2 the increase of crystallites sizes with temperature is parabolic. On the other side, at $T=333$ K, diameters of all crystallites obtained in the range of $J=200$–1000 mA/dm^2 lay inside narrow interval of 18–24 nm.

Due to non-trivial and interdependent influence of T and J on agglomeration, it is difficult to quantitatively analyse parameters of particle distributions presented in Table 3. The existence of three different grain size distributions and significant volume contribution of the LA particles in most of the samples implies that agglomeration is prominent in the entire range of the investigated synthesis conditions, except perhaps for sample 8. General impression is that in the investigated J–T ranges, J influences agglomeration more than T and that at particular T, lower J produces more large-grain particles.

The particles from the "small-grain" (SG) distribution are composed mainly of the WH-phase crystallites. They have larger "asphericity" $|(d-d_{sf})/d|$ than particles from the "intermediate-grain" (IG) distribution, which roughly corresponds to the PL phase and of the "large-agglomerates" (LA) (Table 3). Dimensions and shape of the WH crystallites indicate that they are in the single and/or sub-domain range, and magnetic measurements (Figs. 3 and 5) suggest that they could be in the SPM regime determining the macroscopic magnetic characteristics of the samples. Nevertheless, the SG particles are an order of magnitude larger than the crystallites obtained by XRD and TEM measurements (Table 2), and several times larger than the average particle dimensions determined by SEM, indicating that they are also a product of the initial agglomeration steps. The SG particles prevail in samples 3, 4, 6, and 7, while in sample 5, and samples 1, 2, and 8, obtained under boundary synthesis conditions, the IG particles are favoured. Only sample 5 has no SG particles, implying that under the synthesis conditions $T=333$ K and $J=300$ mA/dm^2, agglomeration is particularly prominent. Yet, at $T=333$ K and higher current densities ($J=500$ mA/dm^2 and 1000 mA/dm^2), agglomeration is weak and(or) slow and a high amount of SG particles is formed. Dimensions of the LA particles of sample 6 are in-between the IG and the LA particles dimensions of other samples, indicating that its synthesis conditions ($T=333$ K and $J=500$ mA/dm^2) might represent a "boundary" case for agglomeration of LA particles. In all of the samples the SG and the IG distributions are quite wide ($\Delta d/d \sim 20$–30%) implying that agglomeration is accompanied by the grain growth, and the LA distribution is narrow ($\Delta d/d \leq 10\%$). In the sample 8, the SG and the IG distributions are narrow, while the LA is completely missing, indicating that processes that took place during the synthesis of sample 8 were very fast and ultimately led to the powder with distinct properties. The presented results suggest that the average grain size of a particular distribution is not determined by growth of smaller grains (this process influences the distribution width, the SG in particular), but by fusion of smaller grains already formed, when the necessary conditions in the EC cell (number, size and shape of grains, J and T) are fulfilled. The SG grains are formed from the initial crystallites, the IG from the SG grains, and the LA from the IG, and perhaps some SG grains, implying that grains of the obtained powders should be self-similar in some respect.

Presence of the LA particles after the 10 min treatment in the ultrasonic bath indicates that interparticle interactions in the powders are quite strong. Immediately after the ultrasonic treatment, the share of SG particles in the suspension varies widely for the samples obtained under various conditions. After 4 days, most of the larger particles segregate, and the SG represents more than 95% of the particles in the suspension.

The shape of the obtained $\chi_N(T)$ characteristics and the position of the maximum is similar for heating in argon (Fig. 3(b)) and in air (Fig. 3(a)), pointing out to the similarities of the initial steps of the magnetic structure reordering during the heating in the two atmospheres. A similar $\chi_N(T)$ characteristic and lowering of T_C on cooling is also observed for magnetite nano-powders in [40], and assigned to a T-dependent interparticle interaction. Besides the C–V redistribution, heating can induce changes of the grain size and shape, influencing that way not only the magnetic domain structure of the samples, but also intra- and interparticle magnetic interactions. This effect could be particularly prominent if the mean value of the grain size distribution is close to one of the "critical" dimensions. An estimate of the critical size for the multi-domain (MD) to single-domain (SD) transition in magnetite is 75 nm [41]. For an ideal spherical particle critical size is 128 nm [42]. The SPM regime at RT is expected for particles with diameter below 30 nm [43]. The crystallite sizes of the investigated powders are well below the SPM limit and the grain sizes before agglomeration are mainly in the range 30–150 nm that covers the MD–SD transition region. Therefore, it could be expected that moderate changes of the grain size and morphology can induce sizable effects in powders macroscopic magnetic properties. The observed fluctuations of $\chi_N(T)$ are most likely induced by the C–V redistribution during the attempt of the system to find a compromise between the structural optimisation (which prefers smaller Fe ions in the LS configuration) and the magnetic order (which favours larger Fe ions in the HS configuration). The $\chi_N(T)$ enhancement observed after the heating/cooling cycle in argon could be related to improvement of the grain microstructure [44], as detected by XRD (Fig. 1), and to better ordering of magnetic moments induced by heating. However, slightly lower T_C observed after cooling suggests that magnetic interaction in the sample is somewhat weaker, probably because the distribution of cations gradually changes from the inverse toward the "random" spinel. The C–V reordering occurs also during the initial stage of heating in air, and it is followed by oxidation that leads to phase transition from magnetite to maghemite.

Further heating in air induces the topotactic phase transformation of ferrimagnetic γ-Fe$_2$O$_3$ to weakly anti-ferromagnetic α-Fe$_2$O$_3$ which results from the rearrangement of small Fe^{3+} ions (Table 2) inside the relatively stable O-matrix, with the plate-like haematite crystallites growing inside the γ-Fe$_2$O$_3$ phase [7]. It usually starts around $T_{inv} \sim 623$ K [7], but can vary over a broad temperature interval (523–1173 K), depending on the initial maghemite structure, particle size, and the conditions of the transition [7,45]. Curie temperature of γ-Fe$_2$O$_3$ is highly uncertain and influenced by numerous factors [16,28,46]. A low T_C is often attributed to a random distribution of vacancies [47], and high T_C values are ascribed to the specific vacancy distribution that maximises the number of paths with strongest magnetic interaction (vacancies are usually placed exclusively at 16d position [46]). The transformation of all γ-Fe_2O_3 phases (face centred cubic, primitive cubic, and tetragonal [16,47–49]) to rombohedral α-Fe_2O_3 is completed bellow their Curie temperatures ($T_{inv} < T_C$), so T_C measurement of γ-Fe_2O_3 is possible only when the phase transition proceeds slower than the thermal demagnetisation. The heating–cooling rate ($\sim$25 K/min^{-1}) applied in this work was rather high, and some γ-Fe_2O_3 that persisted in the newly formed α-Fe_2O_3 phase (see Fig. 3(a) and Fig. 4), offers the possibility to determine T_C of γ-Fe_2O_3. The high T_C value derived ($\approx$ 893 K), together with characteristic super-structure reflections identified in some of the XRD spectra, suggests a specific C–V ordering in the produced maghemite phase.

The temperature induced C–V redistribution in magnetite can happen due to the electron hopping between differently charged Fe ions at 16d, or between 8a and 16d crystallographic positions, and by Fe ions intra-, or inter-site diffusion. In a pure magnetite monocrystal the 16d intra-site electron hopping has the activation energy of about 0.1 eV [33] and is responsible for its high electrical conductivity above the Verwey transition ($T_v \approx 120$ K). The electron hopping between 16d and 8a positions is much less probable, with activation energy between 1.5 and 2.2 eV [48].

In Fig. 6 one can see that heating initially leads to a rapid decrease of $\rho(T)$, both in air and in argon atmosphere, suggesting that in the first stage heating improves the grains microstructure and facilitates electron hopping between Fe^{3+} and Fe^{2+}, most likely by increasing the number of Fe^{3+} at the expense of Fe^{2+} at 16d position, which is indicated also by the $\chi_N(T)$ results. The e-hopping frequency increases to preserve the equilibrium average $Fe^{2.5+}$ charge required at 16d position, thus inducing the observed resistivity decrease. However, activation of longer e-hoping paths at elevated temperatures, including those between the 16d and 8a positions, and a net increase of number of Fe ions at the larger size 16d position (Table 2), should be considered, as well. After initial decrease, formation of maghemite phase leads to a fast increase of $\rho(T)$ for more than six orders of magnitudes. No increase of $\rho(T)$ has been detected during the heating in argon, suggesting that magnetite phase is preserved in the entire temperature interval $270\text{ K} \leq T \leq 620\text{ K}$. After the first heating cycle in argon (Fig. 6 case II) $\rho(T)$ is irreversible on cooling (hysteresis appears), indicating that the heat induced C–V reordering is permanent. Further heating–cooling cycles in argon (Fig. 6 (III)) do not produce significant changes of $\rho(T)$. The dependence is reversible (without hysteresis), in a good agreement with the $\chi_N(T)$ results. The $\rho(T)$ activation energy $E_a = 0.68$ eV obtained from the first heating in argon (Fig. 6 (II)), could be considered as a measure of the irreversible C–V reordering, which takes place also during the initial stage of heating in air, and includes both e-hopping and Fe-diffusion. This energy is considerably higher than the E_a obtained from the second heating in argon ($E_a = 0.23$ eV, Fig. 6(III)), and closer to the E_a obtained from the heating in air ($E_a = 0.98$ eV, Fig. 6(I)), which implies that during the second heating in argon only the low energy e-hopping process takes place. Heating in air induces both the C–V reordering, and maghemite formation through the iron diffusion toward the surface, the complete Fe^{2+} to Fe^{3+} conversion, and Fe reaction with atmospheric oxygen, yields the difference of activation energies of case (I) and case (II) in Fig. 6. It appears that oxidation alone requires less energy than the C–V reordering, but much more than e-hopping.

DC resistivity of pure, stoichiometric magnetite at *RT* is of order of $10^{-2}\,\Omega\,\text{cm}$ [46], and strongly depends on size, structure quality, and history of the sample. In spite of extensive investigations [32–38,48], some doubts [49–51] about magnetite band structure, charge distribution, and nature of its conductivity are still present. After the initial changes during the heating in argon, the investigated samples show a reversible $\rho(T)$ dependence, typical for semiconductors, which allows to relate the activation energy E_a=0.23 eV, to a half of the band-gap energy [33]. This value is higher than $E_a = 0.1$ eV for an ideal magnetite monocrystal, but it is well known that band gap of nano-crystalline semiconductors strongly depends on crystallite size and shape, and structure quality [32–38,42].

5. Conclusions

Characteristics of magnetite nano-sized powders obtained by electrochemical synthesis under various conditions, the influence of heating and oxidation on their properties, the magnetite to maghemite, and the maghemite to haematite phase transitions have been investigated by extensive measurements. It has been established that both hydrogen and water promotes in-situ formation and stabilisation of magnetite during the EC synthesis, and that is possible to adjust the grain size and shape, and electrical and magnetic characteristics of the powders using the appropriate synthesis conditions and the subsequent thermal treatment. Under investigated synthesis conditions, temperature T influences the crystallite size more than current density J, but J has a larger impact on agglomeration. The produced powders are composed of the two quite different phases, originating from the corresponding precursor hydroxides. The nanometre-size, needle like crystallites (whiskers) and their bundles originate from goethite, they are superparamagnetic at *RT*, and dominate the macroscopic magnetic properties of the samples. The large, plate-like grains originate from lepidocrocite, and the results suggest that most of them have a pseudo single-domain rather than a multi-domain magnetic structure.

The first non-isothermal heating in argon induces the irreversible process of cation and vacancy (C–V) reordering, which leads to increase of conductivity and magnetisation of the samples. The reordering is influenced by two competing tendencies: the tendency of the structure to accommodate smaller Fe ions with valence closer to Fe^{3+} and(or) those in the low-spin state, and the tendency of the cation subsystem to maximise the magnetic interaction, promoting the Fe ions into the high-spin state, and favouring their distribution with maximal number of paths with the strongest exchange interaction. Repeated heating/cooling in argon induces only reversible changes of $\chi_N(T)$ and $\rho(T)$, indicating that the configuration reached during the C–V reordering is stable in the considered temperature range. During heating in air, the C–V reordering is accompanied by oxidation, and around 600 K the maghemite phase appears with an abrupt increase of electrical resistivity for six orders of magnitude. The C–V reordering has higher activation energy than oxidation alone, but they both considerably exceed the energy of electron hopping, though all processes are highly correlated. The specific C–V ordering is responsible also for formation of the maghemite superstructure phase with high Curie temperature of about 893 K. Further heating in air leads to the γ-Fe_2O_3 to α-Fe_2O_3 phase transition which is particularly prominent above 600 K.

The obtained results elucidate the possibilities for production of the magnetite powders with crystallites and grains of particular size and shape by choosing adequate EC synthesis conditions, and their modification by an appropriate heat treatment in a suitable atmosphere. In that way, the powders with a desired magnetite/maghemite/haematite phase content and macroscopic characteristics can be produced in large quantities, and at low cost.

Acknowledgements

This work was supported by Serbian Ministry of Education, Science and Technology under the grant III45003.

References

[1] R.M. Cornell, U. Schwertmann, Iron Oxides, VCH Verlagsgesellschaft, Weinheim, 1996.

[2] L. Neel, Advances in Physics 4 (1955) 191–242.

[3] S.-Y. Chen, A. Gloter, A. Zobelli, L. Wang, C-H. Chen, C. Colliex, Physical Review B 79 (104103) (2009) 1–10.

[4] S. Mørup, Magnetic properties of fine particles, in: J.L. Dormann, D. Fiorani (Eds.), North Holland Delta Series, Amsterdam 1992, pp. 125–190.

[5] C. Boyer, M.R. Whittaker, V. Bulmus, J. Liu, T.P. Davis, NPG Asia Materials 2 (2010) 23–30.

[6] B. Berkovski, V. Bashtovoy (Eds.), Magnetic Fluids and Applications Handbook, Begel House Inc., New York, 1996.

[7] C.B. de Boer, M.J. Dekkers, Geophysical Journal International 144 (2001) 481–494.

[8] M. Bonnin-Mosbah, A.S. Simionovici, N. Métrich, J-P. Duraud, D. Massare, P. Dillmann, Journal of Non-Crystalline Solids 288 (2001) 103–113.

[9] R.L. Frost, Z. Ding, H.D. Ruan, Journal of Thermal Annalyses and Calorimetry 71 (2003) 783–797.

[10] S. Nasrazadani, Corrosion Science 39 (1997) 1845–1859.

[11] A.V. Smirnov, J.A. Tarduno, Earth and Planetary Science Letters 194 (2002) 359–368.

[12] H.V. Lauer, D.W. Ming, D.C. Golden, Lunar and Planetary Science XXXIV (2003) 1341.

[13] S. Lefebvre, E. Dubois, V. Cabuil, S. Neveu, R. Massart, Journal of Materials Research 13 (1998) 2975–2981.

[14] A. Bharde, A. Wani, Y. Shouche, P.A. Joy, B.L.V. Prasad, M. Sastry, Journal of the American Chemical Society 127 (2005) 9326–9327.

[15] M. López-Quintela, J. Rivas, Journal of Colloid and Interface Science 158 (1993) 446–451.

[16] C.J. Goss, Physics and Chemistry of Minerals 16 (1988) 164–171.

[17] T.-Y. Ying, S. Yiacomi, C. Tsouris, Journal of Dispersion Science and Technology 23 (2002) 569–576.

[18] L. Cabrera, S. Gutierrez, N. Menendez, M.P. Morales, P. Herrasti, Electrochemica Acta 53 (2008) 3436–3441.

[19] Ž. Tomić, P. Jovanić, A. Bugarinović, S. Vardić, A. Maričić, Lj. Vulićević, G. Gligorić, Serbian Journal of Electrical Engineering 3 (2004) 29–34.

[20] B.N. Figgis, J. Lewis, in: H.B. Jonassen, A. Weissberger (Eds.), Technique of Inorganic Chemistry, vol. IV, Interscience, New York, 1965, pp. 212–219.

[21] Lj. Vuličević, N. Ivanović, N. Popović, M. Novaković, M. Popović, M. Mitrić, V. Andrić, D. Babić, Journal of Microscopy 232 (2008) 629–633.

[22] M. Friáck, A. Schindlmayer, M. Scheffler, New Journal of Physics 9 (5) (2007) 1–15.

[23] J. Slater, Quantum Theory of Molecules and Solides, vol. 2, MsGrow-Hill, New York, 1965, p. 99.

[24] R.D. Shannon, Acta Crystallographica A 32 (1976) 51–767.

[25] G. Gottstein, Physical Foundations of Materials Science, Springer-Verlag, Berlin Heidelberg, Germany, 2004.

[26] J.P. Sanders, P.K. Gallagher, Journal of Thermal Analysis and Calorimetry 72 (2003) 777–789.

[27] J. Tang, M. Myers, K.A. Bosnick, L.E. Brus, Journal of Physical Chemistry B 107 (2003) 7501–7506.

[28] T.S. Gendler, V.P. Scherbakov, M.J. Dekkers, A.K. Gapeev, S.K. Gribov, E. McClelland, Geophysical Journal International 160 (2005) 815–832.

[29] S. Levi, R.T. Merrill, Journal of Geophysical Research 83 (1978) 309–323.

[30] G.F. Goya, T.S. Berquó, F.C. Foncesa, M.P. Morales, Journal of Applied Physics 94 (2003) 3520–3528.

[31] F. Heider, A. Zitzelsberger, K. Fabian, Physics of the Earth and Planetary Interiors 93 (1996) 239–256.

[32] N. Guskos, G.J. Papadopoulos, V. Likodimis, S. Patapis, D. Yarmis, A. Przpiera, K. Przpiera, J. Majszczyk, J. Typek, M. Wabia, K. Aidinis, Z. Drazek, Materials Research Bulletin 37 (2002) 1051–1061.

[33] J.H. Park, L.H. Tjeng, J.W. Allen, P. Metcalf, C.T. Chen, Physical Review B 55 (1997) 12813–12817.

[34] J.H.V.J. Brabers, F. Walz, H. Kronmueller, Journal of Physics: Condensed Matter 11 (1999) 3679–3684.

[35] S. Dutta, S.K. Manik, M. Pal, S.K. Pradhan, P. Brahma, D. Chakravorty, Journal of Magnetism and Magnetic Materials 288 (2005) 301–306.

[36] L. Wang, J. Li, W. Ding, T. Zhou, B. Liu, W. Zhong, J. Wu, Y. Du, Journal of Magnetism and Magnetic Materials 207 (1999) 111–117.

[37] Y.S. Dedkov, U. Rüdiger, G. Güntherodt, Physical Review B 65 (2002) 064417 (5pp).

[38] A.J.M. Kuipers, V.A.M. Brabers, Physical Review B 14 (1976) 1401–1405.

[39] K.S. Rane, V.M.S. Verenkar, R.M. Pednekar, P.Y. Sawant, Journal of Materials Science: Materials in Electronics 10 (1999) 121–132.

[40] R.N. Panda, N.S. Gajbhiye, G. Balaji, Journal of Alloys and Compounds 326 (2001) 50–53.

[41] H.P. Johnson, R.T Merrill, Journal of Geophysical Research 79 (1974) 5533–5534.

[42] C.M. Sorensen, in: K.J. Klabunde (Ed.), Nanoscale Materials in Chemistry, John Willy & Sons, New York, 2001, p. 201.

[43] J. Lee, T. Isobe, M. Senna, Journal of Colloid and Interface Science 177 (1996) 490.

[44] J.F. Bonfield, P.J. Wasilewski, D.R. Veblen, American Mineralogist 79 (1994) 654–667.

[45] T. Belin, N. Guigue-Millot, T. Caillot, D. Aymes, J.C. Niepce, Journal of Solid State Chemistry 163 (2002) 459–465.

[46] G.M. da Costa, E. De Grave, R.E. Vandenberghe, Hyperfine Interactions 117 (1998) 207–243.

[47] H. Takei, S. Chiba, Journal of the Physical Society of Japan 21 (1966) 1255–1263.

[48] M. Imada, A. Fujimori, Y. Tokura, Reviews of Modern Physics 70 (1998) 1039–1263.

[49] P. Poddar, T. Fried, G. Markovich, Physical Review B 65 (172405) (2002) 1–4.

[50] G. Subías, J. García, J. Blasco, M. Grazia Proietti, H. Renevier, M. Concepción Sánchez, Physical Review Letters 93 (156408) (2004) 1–4.